

Article

## Hydrogen Production from Water by Photolysis, Sonolysis and Sonophotolysis with Solid Solutions of Rare Earth, Gallium and Indium Oxides as Heterogeneous Catalysts

Marta Penconi <sup>1,†</sup>, Federico Rossi <sup>2</sup>, Fausto Ortica <sup>1,2,3,4</sup>, Fausto Elisei <sup>1,2,3</sup>  
and Pier Luigi Gentili <sup>1,2,\*</sup>

<sup>1</sup> Dipartimento di Chimica, Biologia e Biotecnologie, Università di Perugia, Via Elce di Sotto, 8, 06123 Perugia, Italy; E-Mails: fausto.ortica@unipg.it (F.O.); fausto.elisei@unipg.it (F.E.)

<sup>2</sup> Inter-University Research Center on Pollution and Environment “Mauro Felli” (CIRIAF), Via G. Duranti 67, 06125 Perugia, Italy; E-Mail: federico.rossi@unipg.it

<sup>3</sup> Centre of Excellence on Nanostructured Innovative Materials (CEMIN), Università di Perugia, via Elce di Sotto 8, 06123 Perugia, Italy

<sup>4</sup> Istituto Nazionale di Fisica Nucleare (INFN), Sezione di Perugia, Via Pascoli, 06123 Perugia, Italy

<sup>†</sup> Current Affiliation: Istituto di Scienze e Tecnologie Molecolari del CNR (CNR-ISTM), via C. Golgi 19, 20133 Milano, Italy; E-Mail: marta.penconi@alice.it.

\* Author to whom correspondence should be addressed; E-Mail: pierluigi.gentili@unipg.it; Tel.: +39-075-585-5573; Fax: +39-075-585-5598.

Academic Editor: Marc A. Rosen

Received: 18 May 2015 / Accepted: 10 July 2015 / Published: 16 July 2015

---

**Abstract:** In this work, we present the hydrogen production by photolysis, sonolysis and sonophotolysis of water in the presence of newly synthesized solid solutions of rare earth, gallium and indium oxides playing as catalysts. From the experiments of photolysis, we found that the best photocatalyst is the solid solution  $Y_{0.8}Ga_{0.2}InO_3$  doped by sulphur atoms. In experiments of sonolysis, we optimized the rate of hydrogen production by changing the amount of water, adding ethanol and tuning the power of our piezoelectric transducer. Finally, we performed sonolysis and sonophotolysis experiments in the presence of  $S:Y_{0.8}Ga_{0.2}InO_3$  finding a promising synergistic effect of UV-visible electromagnetic waves and 38 kHz ultrasound waves in producing  $H_2$ .

**Keywords:** hydrogen energy; solar energy; photocatalysis; sonochemistry; synergy; metal oxides; sulphur-doping

---

## 1. Introduction

Hydrogen is considered a promising energy vector for the next generations. It can be used for supplying “green” electricity production or cogeneration systems such as fuel cells [1–7]. The sustainability of its employment depends on the energy source used to synthesize it from hydrogen-rich compounds such as water or biomass. The splitting of water in hydrogen and oxygen by means of solar radiation is one of the most attractive methods [8–12]. Water splitting is not an easy process—suffice it to think that the overall reaction requires a free energy of 237 kJ/mol in standard conditions. Moreover, pure water absorbs only few IR frequencies of the solar spectrum reaching the biosphere and such IR radiation is not enough to dissociate water molecules. Therefore, we need a photocatalyst to achieve water splitting by solar radiation, *i.e.*, a species that absorbs photons of higher energy and triggers the redox elementary steps required to break H<sub>2</sub>O in H<sub>2</sub> and O<sub>2</sub>. Among the many possible photocatalysts, heterogeneous metal oxides are particularly appealing due to their stability and endurance to photo-corrosion. Metal oxides are often semiconductors that absorb solar photons with energy equal to or higher than their band gaps. The absorption of photons causes the jump of electrons from the valence band (VB) to the conduction band (CB), leaving positive holes in the VB. Positive and negative charges must, then, reach the surface of the particles without recombining each other and promote the oxidation of oxygen and the reduction of hydrogen, respectively. Hydrogen reduction is thermodynamically feasible if the electric potential associated with electrons in the conduction band is more negative than the redox potential of H<sup>+</sup>/H<sub>2</sub>, whereas holes in the valence band oxidize oxygen of water if their potential is more positive than that of the pair O<sub>2</sub>/H<sub>2</sub>O. These thermodynamic requirements impose the employment of large band gap semiconductors, absorbing only in the UV, with a consequent waste of a broad portion of solar spectrum. However, when the goal is just the photo-production of hydrogen from water, even visible-light-response semiconductors can be used as long as they work in the presence of a sacrificial reagent, *i.e.*, a chemical species that can be oxidized more easily than the oxygen of water [13]. This strategy is quite attractive, especially when the sacrificial reagent is a biomass compound, such as ethanol generated by fermentation of sugars [14]. Band gap engineering is the right way to obtain semiconductors having both narrow band gaps and a highly negative electric potential associated with their conduction bands. This may be achieved through the synthesis of solid solutions combining wide and narrow band gap semiconductors; the electric potential of the conduction and valence bands can be tuned by varying the stoichiometry of the photocatalyst [15–18]. To reduce the band gap of a metal oxide semiconductor, the valence band can be extended by doping with nitrogen or sulphur atoms [19–21]. If, after the preparation of the solid solutions, there is still a broad portion of solar spectrum that is not absorbed, it is anyway possible to avoid the complete waste of low frequencies of the solar spectrum through the up-conversion process [22–25].

A promising methodology to improve the efficiency of the hydrogen production from water consists in merging heterogeneous photocatalysis and sonochemistry. Ultrasound waves trigger chemical reactions through the acoustic cavitations, which are non-linear acoustic phenomena that occur in a liquid when irradiated with high power and low frequencies (20–100 kHz) ultrasounds. Acoustic cavitations give rise to extraordinary power densities in a small volume and over an extremely short time, providing favorable conditions for high-temperature and/or high-pressure chemical reactions [26]. In heterogeneous systems, the presence of a solid phase promotes sonochemical processes, since the solid particles dispersed in the liquid and the trapped gas in the crevices play as nuclei for the concentration of the acoustic energy. It derives that sonophotocatalysis is used for degradation of organic pollutants in water [27] and in the ultrasound-assisted photocatalysis for hydrogen production from water [14,28,29]. The simultaneous use of light and ultrasound irradiation often exhibits an interesting synergistic effect [29–37].

In this study, we compare the photo-production of hydrogen by four solid solutions having  $\text{Ln}_{0.8}\text{Ga}_{0.2}\text{InO}_3$  as the general formula, with Ln = La, Gd, Y, Yb, both undoped and doped with sulphur atoms. This comparison is useful to pinpoint the best lanthanide among the four we have chosen, knowing that all of them assure a very negative contribution to the conduction band flat potential of the synthesized semiconductor photocatalysts.

For the most active photocatalyst, that is, S:Y<sub>0.8</sub>Ga<sub>0.2</sub>InO<sub>3</sub>, we present the results of sonolysis and sono-photolysis experiments. The sonolysis experiments have been performed after optimizing the power of the piezoelectric transducer, the composition and the volume of the liquid. Finally, the hybrid action of UV-visible electromagnetic radiation of 38 kHz ultrasound waves shows a promising synergistic effect.

## 2. Experimental Section

### 2.1. Chemicals

The chemicals, Ga<sub>2</sub>O<sub>3</sub> (grade >99.99%), In<sub>2</sub>O<sub>3</sub> (grade 99.999%), La<sub>2</sub>O<sub>3</sub> (grade 99.999%), Y<sub>2</sub>O<sub>3</sub> (grade 99.999%), Gd<sub>2</sub>O<sub>3</sub> (grade >99.99%), Yb<sub>2</sub>O<sub>3</sub> (grade 99.99%), thiourea (H<sub>2</sub>NCSNH<sub>2</sub>) (grade ≥99.0%), potassium iodide (KI) (grade >99.99%) and ethanol (grade >99.8%), were supplied by Sigma-Aldrich and used without further purification. Water was deionized and distilled before use.

### 2.2. Preparation and Characterization of Photocatalysts

The solid solutions, having general formula  $\text{Ln}_{0.8}\text{Ga}_{0.2}\text{InO}_3$  (with Ln = La, Gd, Y, Yb), were prepared at high temperature through acid-base reactions with the metal oxides In<sub>2</sub>O<sub>3</sub>, Ga<sub>2</sub>O<sub>3</sub> and Ln<sub>2</sub>O<sub>3</sub> as reagents. The reagents in the appropriate molar ratios were mixed and grounded by a miller. Then, the mixture of solids was sintered at 1373 K for 24 hours inside a muffle furnace under aerated conditions.

To dope the photocatalysts by sulphur atoms the prepared  $\text{Ln}_{0.8}\text{Ga}_{0.2}\text{InO}_3$  solid solutions were mixed with thiourea in a 1:4 molar ratio. The mixture was heated at 773 K under aerated conditions for 5 hours. After cooling, the powder was washed with double distilled water and dried.

We recorded UV-visible reflectance spectra of the powdery samples by a portable spectrophotometer with a deuterium–halogen lamp (AvaLight-D(H)-S) as excitation source, an

integrating sphere with a 6-mm diameter viewing aperture (AvaSphere-30-refl), a high-sensitivity Avantes Charge-Coupled Device (CCD) detector (86 photons/count, 200–1100 nm, grating 300 lines/mm), connected through a fiber optic system. The reflectance spectra were transformed in Kubelka-Munk units according to Equation (1) [38]:

$$\frac{K}{S} = \frac{[1 - R_{\lambda_0}]^2}{2R_{\lambda_0}} = F(R_{\lambda_0}) \quad (1)$$

where  $K$  and  $S$  are the wavelength-dependent apparent absorption and scattering coefficients;  $R_{\lambda_0}$  is the reflectance value experimentally recorded at  $\lambda_0$  and  $F(R_{\lambda_0})$  is the so-called re-emission function at  $\lambda_0$ . The band gap energies of the semiconductors have been determined by calculating the first derivatives of the spectra. By plotting  $dF(R_{\lambda_0})/d\lambda$  as a function of  $\lambda$ , the band gap transitions give rise to negative bands with a maximum at the inflection point. After describing these bands with Gaussian functions, we fixed the wavenumber of their centers as the best estimate of the band gap.

X-ray diffraction spectra were recorded through a Philips X'PERT PRO diffractometer with  $\text{CuK}\alpha$  radiation.

### 2.3. Sonophotocatalytic Experiments

The details of the experimental setup, employed to carry out the experiments of photocatalysis, sonocatalysis and sonophotocatalysis, have been described elsewhere [29]. Herein, we describe the main properties. The source of ultrasounds is located at the bottom side of the reactor; it consists of a piezoelectric transducer, producing mechanical waves of 38 kHz at 50 W. For the photolysis experiments, a Sun 2000 Abet Solar Simulator (model LSO 100) equipped with a 500 W Xenon lamp has been employed as source of electromagnetic radiation. The powdery catalyst was suspended in water/ethanol solutions and inserted into the reactor. The free volume inside the reactor was filled with argon at the pressure of 1 bar. The system was thermostated at 298 K. Temperature and pressure inside the reactor were constantly monitored through a thermocouple located at the half height of the aqueous solution and a pressure probe, respectively.

The amount of evolved hydrogen was measured by a gas-chromatograph (CP-4900, Varian) equipped with a molecular sieve column and a thermal conductivity detector. The experiments for the different samples have been repeated at least twice. The uncertainties in the amounts of hydrogen have been determined by calculating their standard deviations. The acoustic power (PUS) dissipated into the liquid by the piezoelectric transducer, was estimated by calorimetric measurements and calculated using Equation (2) [39]:

$$P_{US} = m \cdot C_P \left( \frac{dT}{dt} \right) \quad (2)$$

where  $m$ ,  $C_P$  and  $dT/dt$  are the mass of water (expressed in g), the heat capacity of water at constant pressure ( $4.2 \text{ J}\cdot\text{K}^{-1}\cdot\text{g}^{-1}$ ) and the rate of temperature increase per second, respectively. The measurement of the acoustic power was carried out in 100 mL of double distilled water and we found an average value of 2.6 W, which corresponds to a power density of  $26 \text{ W}/\text{dm}^3$ . We repeated the calorimetric determination at least three times.

In order to calculate the sonochemical efficiency (SE) of the reactor, the oxidation of potassium iodide was chosen as chemical dosimeter [39]. Under ultrasound irradiation of an aqueous solution of KI, the generated  $\bullet\text{OH}$  radical oxidizes  $\text{I}^-$  ions to yield  $\text{I}_2$ . The excess of  $\text{I}^-$  ions in solutions reacts with  $\text{I}_2$  to give  $\text{I}_3^-$  ions. The amount of  $\text{I}_3^-$  ions produced was evaluated by UV spectrophotometry measuring the absorbance at 355 nm ( $\epsilon = 26,303 \text{ dm}^3 \cdot \text{mol}^{-1} \cdot \text{cm}^{-1}$ ). The measurement was carried out by irradiating 100 ml of an aqueous solution of KI 0.1 M for 30 min. The sonochemical efficiency (SE) of the reactor is defined as the ratio of the  $\text{I}_3^-$  moles produced by KI dosimetry to the ultrasound energy  $E_{US}$  according to Equation (3):

$$SE = \frac{\text{mol}(\text{I}_3^-)}{E_{US}} = \frac{[\text{I}_3^-] \cdot V}{P_{US} \cdot t} \quad (3)$$

where  $[\text{I}_3^-]$ ,  $V$ ,  $P_{US}$  and  $t$  are the concentration of the  $\text{I}_3^-$  ions, the irradiated volume of KI solution, the acoustic power estimated by calorimetry and the irradiation time, respectively. Thus, the calculated SE of  $1.5 \times 10^{-10} \text{ mol} \cdot \text{J}^{-1}$  corresponds to the moles of  $\text{I}_3^-$  produced per unit of time by the sonochemical reaction normalized by the absorbed ultrasonic energy.

### 3. Results and Discussion

#### 3.1. Synthesis and Characterization of the Photocatalysts

The samples  $\text{Ln}_{0.8}\text{Ga}_{0.2}\text{InO}_3$  (with Ln = La, Gd, Y, Yb) were prepared through solid state reactions after mixing the metal oxides  $\text{Ln}_2\text{O}_3$ ,  $\text{Ga}_2\text{O}_3$  and  $\text{In}_2\text{O}_3$  in the right molar ratio (see the Experimental Section). We have chosen the stoichiometry  $\text{Ln}_{0.8}\text{Ga}_{0.2}\text{InO}_3$  because when Ln was La, it resulted in the most active photocatalyst within a series of materials having  $\text{La}_{2x}\text{Ga}_{2y}\text{In}_{2z}\text{O}_3$  as general formula [37]. The X-ray diffraction (XRD) patterns of  $\text{Ln}_{0.8}\text{Ga}_{0.2}\text{InO}_3$  are reported in Figure 1A.  $\text{La}_{0.8}\text{Ga}_{0.2}\text{InO}_3$  [37] is a composite material consisting of three distinct phases (see the first XRD pattern from top of Figure 1A). First, the distorted perovskite  $\text{LaInO}_3$  structure being composed of tilted octahedral  $\text{InO}_6$ , with  $\text{La}^{+3}$  ions lying intermediate between neighboring octahedra. It has an orthorhombic symmetry [40,41] and its XRD pattern presents a characteristic triplet signal centered at  $30.74^\circ$  (its peaks have been labeled as  $o_1$  in Figure 1). The formation of ternary solid solution can be inferred from the slight shift towards greater values of reflection angles compared to those typical of the pure  $\text{LaInO}_3$  binary oxide. Such shifts are due to the substitution of  $\text{In}^{+3}$  with the smaller  $\text{Ga}^{+3}$  ions. The second phase is a cubic crystal structure derived from that of  $\text{In}_2\text{O}_3$  (indicated in Figure 1 by the letter c). Finally, there is the third and less abundant phase, that is  $\text{LaGaO}_3$  (its peaks have been labeled as  $o_2$  in Figure 1), whose most intense peak is at  $32.4^\circ$  rather than at  $32.6^\circ$ , due to a partial replacement of  $\text{Ga}^{+3}$  with larger  $\text{In}^{+3}$  ions.

The substitution of lanthanum with the other rare earth ions determines the appearance of new phases deriving from the binary oxides  $\text{GdInO}_3$ ,  $\text{YInO}_3$  and  $\text{YbInO}_3$ , that crystallize in a non-centrosymmetric hexagonal structure with space group  $\text{P6}_3\text{cm}$  [42–44]. The hexagonal structure (whose peaks have been labeled as h in Figure 1) consists of  $\text{InO}_5$  trigonal bipyramids. The bases of the pyramids are corner linked to form a triangular lattice in the basal plane. A layer of  $\text{Ln}^{+3}$  separates the layers of corner-shared trigonal bipyramids. The  $\text{In}^{+3}$  ions are fivefold-coordinated in the trigonal

bipyramidal site, while the  $\text{Ln}^{+3}$  ions are seven-fold coordinated. The presence of the cubic phase can be ascertained in all the samples (see the peaks labeled by c in Figure 1A).

When the solid solutions  $\text{Ln}_{0.8}\text{Ga}_{0.2}\text{InO}_3$  were sulphur-doped, we did not see relevant modification in the crystal structures. The relative intensities of the peaks in our diffractograms change after doping our samples because sulphur atoms dope the different phases in distinct manner. In fact, their XRD diffractograms (see Figure 1B) showed the same diffraction peaks, although the relative intensities were quite different.

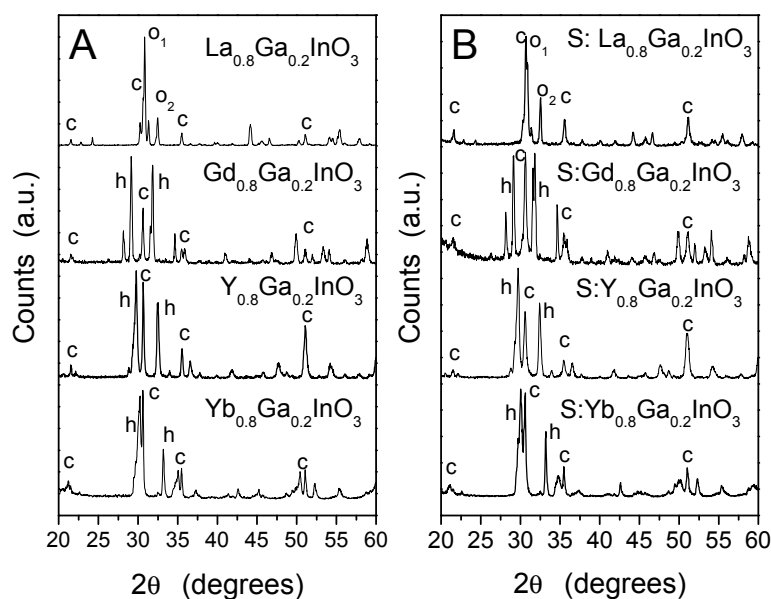


**Figure 1.** X-ray diffraction spectra of the solid solutions (A) undoped:  $\text{La}_{0.8}\text{Ga}_{0.2}\text{InO}_3$ ,  $\text{Gd}_{0.8}\text{Ga}_{0.2}\text{InO}_3$ ,  $\text{Y}_{0.8}\text{Ga}_{0.2}\text{InO}_3$ ,  $\text{Yb}_{0.8}\text{Ga}_{0.2}\text{InO}_3$ , and (B) sulphur-doped:  $\text{S}:\text{La}_{0.8}\text{Ga}_{0.2}\text{InO}_3$ ,  $\text{S}:\text{Gd}_{0.8}\text{Ga}_{0.2}\text{InO}_3$ ,  $\text{S}:\text{Y}_{0.8}\text{Ga}_{0.2}\text{InO}_3$ ,  $\text{S}:\text{Yb}_{0.8}\text{Ga}_{0.2}\text{InO}_3$ . The peaks corresponding to the cubic phase are labeled by c.

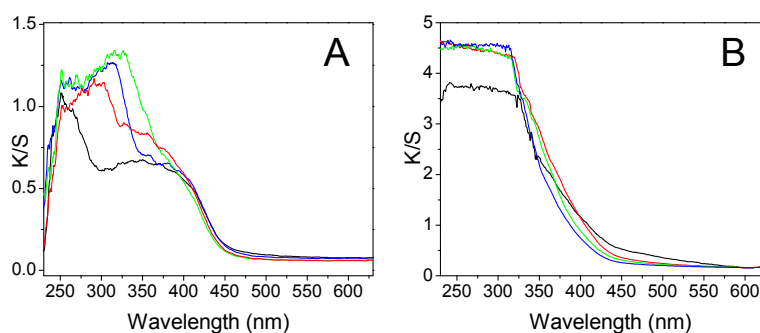


**Figure 2.** Absorption spectra of the solid solutions (A) undoped:  $\text{La}_{0.8}\text{Ga}_{0.2}\text{InO}_3$  (black)  $\text{Gd}_{0.8}\text{Ga}_{0.2}\text{InO}_3$  (blue),  $\text{Y}_{0.8}\text{Ga}_{0.2}\text{InO}_3$  (red) and  $\text{Yb}_{0.8}\text{Ga}_{0.2}\text{InO}_3$  (green); (B) sulphur-doped:  $\text{S}:\text{La}_{0.8}\text{Ga}_{0.2}\text{InO}_3$  (black),  $\text{S}:\text{Gd}_{0.8}\text{Ga}_{0.2}\text{InO}_3$  (blue),  $\text{S}:\text{Y}_{0.8}\text{Ga}_{0.2}\text{InO}_3$  (red) and  $\text{S}:\text{Yb}_{0.8}\text{Ga}_{0.2}\text{InO}_3$  (green).

The UV-visible absorption spectra in Kubelka-Munk units of the  $\text{Ln}_{0.8}\text{Ga}_{0.2}\text{InO}_3$  solid solutions are depicted in Figure 2A. All the samples showed the edge of absorption in the visible region due to the indium oxide cubic phase. Its band gap is slightly different in each sample (see Table 1). The tiny

differences are due to the different  $\text{Ln}^{+3}$  ions present in the four cubic phases. Although the cubic phase of  $\text{In}_2\text{O}_3$  guarantees the red shift in the absorption spectra, it is not suitable by itself to produce hydrogen from water by photocatalysis because its redox potential of the conduction band is not sufficiently negative [37].

The data in Table 1 show that  $\text{Gd}_{0.8}\text{Ga}_{0.2}\text{InO}_3$  and  $\text{La}_{0.8}\text{Ga}_{0.2}\text{InO}_3$  have slightly narrower band gaps than  $\text{Y}_{0.8}\text{Ga}_{0.2}\text{InO}_3$  and  $\text{Yb}_{0.8}\text{Ga}_{0.2}\text{InO}_3$ . The red-shift that is evident into the UV region is due to the different chemical composition of the solid solutions of oxides.

**Table 1.** Band gaps (expressed in eV and nm) of the cubic phase for the undoped solid solutions  $\text{Ln}_{0.8}\text{Ga}_{0.2}\text{InO}_3$ .

Sample	BG, eV (nm)
$\text{La}_{0.8}\text{Ga}_{0.2}\text{InO}_3$	2.93 (423)
$\text{Gd}_{0.8}\text{Ga}_{0.2}\text{InO}_3$	2.92 (425)
$\text{Y}_{0.8}\text{Ga}_{0.2}\text{InO}_3$	2.95 (420)
$\text{Yb}_{0.8}\text{Ga}_{0.2}\text{InO}_3$	2.96 (419)

The doping by sulphur atoms increased the probability of absorption of UV and blue radiation by our photocatalysts, but it did not change their band gaps (see Figure 2B).

### 3.2. Hydrogen Production by Photocatalysis

In a typical photolysis experiment, 0.4 g of photocatalyst were suspended in 300 ml of a mixture ethanol/water (20% vol). The suspension was irradiated by the solar simulator at  $1000 \text{ W/m}^2$ . Our photocatalysts work well if we do not exclude UV radiation. We checked the progress of the photocatalytic reactions by gas chromatography (see the Experimental Section). The amount of hydrogen produced at different irradiation times are plotted in Figure 3. Figure 3A shows the hydrogen produced by the undoped solid solutions  $\text{Ln}_{0.8}\text{Ga}_{0.2}\text{InO}_3$  in six hours of irradiation. The best photocatalyst was  $\text{Y}_{0.8}\text{Ga}_{0.2}\text{InO}_3$  producing  $0.63 \mu\text{moles}$  of  $\text{H}_2$  after six hours. The amount of  $\text{H}_2$  obtained with  $\text{Y}_{0.8}\text{Ga}_{0.2}\text{InO}_3$  is almost twofold larger than that achieved with  $\text{La}_{0.8}\text{Ga}_{0.2}\text{InO}_3$ . Anyway, it is worthwhile noticing that such amounts are not remarkable because our reactor has been optimized to perform sono-photolysis experiments and not simply photolysis experiments. In fact, if the piezoelectric transducer is switched off, there are no ultrasound waves within the reactor and the particles of the catalysts settle down on the bottom part of the reactor. Nevertheless, we may state that  $\text{Y}_{0.8}\text{Ga}_{0.2}\text{InO}_3$  is a promising photocatalyst. In fact, in our device it showed better performances than  $\text{La}_{0.8}\text{Ga}_{0.2}\text{InO}_3$ , and  $\text{La}_{0.8}\text{Ga}_{0.2}\text{InO}_3$  showed to be more active [29] than the well-known  $\text{GaInO}_3$  having Pt as cocatalyst [15] and  $\text{TiO}_2$ . Moreover, our photocatalysts did not show any sign of degradation.

The photocatalytic hydrogen production by the sulphur-doped solid solutions are shown in Figure 3B. If we make a list of the efficiency of the sulphur-doped photocatalysts, we ascertain that, again, on top there is the material having Y as rare earth ion: S: $\text{Y}_{0.8}\text{Ga}_{0.2}\text{InO}_3$ . Then, the photocatalyst with La follows, *i.e.*, S: $\text{La}_{0.8}\text{Ga}_{0.2}\text{InO}_3$ . At the bottom of the list, we have the solid solutions with Gd and Yb, *i.e.*, S: $\text{Gd}_{0.8}\text{Ga}_{0.2}\text{InO}_3$  and S: $\text{Yb}_{0.8}\text{Ga}_{0.2}\text{InO}_3$ .

The rates of  $\text{H}_2$  production for all the materials we synthesized are reported in Table 2. All the photocatalysts had micrometric particles as revealed by scanning electron microscopy. From the data

of Table 2, it is evident that the sulphur-doping always increases the photocatalytic activity. Such an effect is more pronounced on  $Y_{0.8}Ga_{0.2}InO_3$  that becomes seven times more active. The material S: $Y_{0.8}Ga_{0.2}InO_3$  guaranteed the maximum value of the rate of  $H_2$  production, that is one  $\mu$ mole per hour.

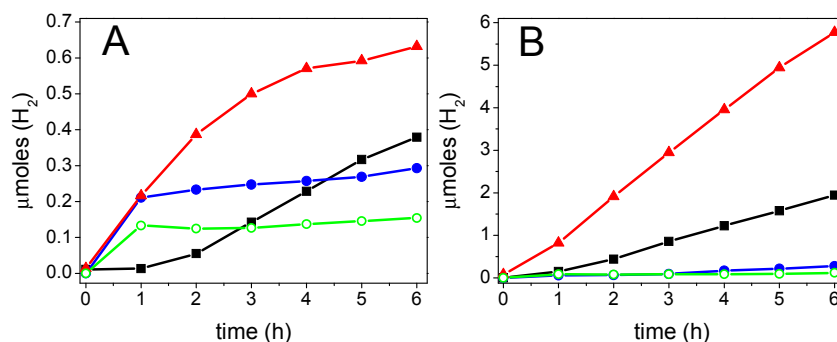


**Figure 3.** Hydrogen production ( $\mu$ moles) as a function of time (hours) determined in photolysis experiments in a suspension of 0.4 g of photocatalyst in 300 ml ethanol/water (20 vol%) irradiated by the solar simulator. **(A)** Undoped solid solutions:  $La_{0.8}Ga_{0.2}InO_3$  (black squares),  $Gd_{0.8}Ga_{0.2}InO_3$  (blue circles),  $Y_{0.8}Ga_{0.2}InO_3$  (red triangles) and  $Yb_{0.8}Ga_{0.2}InO_3$  (green open circles). **(B)** Sulphur-doped solid solutions: S: $La_{0.8}Ga_{0.2}InO_3$  (black squares), S: $Gd_{0.8}Ga_{0.2}InO_3$  (blue circles), S: $Y_{0.8}Ga_{0.2}InO_3$  (red triangles) and S: $Yb_{0.8}Ga_{0.2}InO_3$  (green open circles).

**Table 2.** Rates of  $H_2$  production ( $\mu$ moles/h) for the undoped and sulphur-doped solid solutions in a suspension of 0.4 g of photocatalyst in 300 ml ethanol/water (20 vol%) irradiated by the solar simulator. The uncertainties have been calculated as standard deviations of measurements repeated by using catalysts obtained through distinct synthesis.

Undoped Solid Solutions		Sulfur-Doped Solid Solutions	
Sample	$\mu$ moles ( $H_2$ )/h	Sample	$\mu$ moles ( $H_2$ )/h
$La_{0.8}Ga_{0.2}InO_3$	$0.08 \pm 0.03$	S: $La_{0.8}Ga_{0.2}InO_3$	$0.36 \pm 0.10$
$Gd_{0.8}Ga_{0.2}InO_3$	$0.015 \pm 0.006$	S: $Gd_{0.8}Ga_{0.2}InO_3$	$0.045 \pm 0.02$
$Y_{0.8}Ga_{0.2}InO_3$	$0.14 \pm 0.05$	S: $Y_{0.8}Ga_{0.2}InO_3$	$1.0 \pm 0.4$
$Yb_{0.8}Ga_{0.2}InO_3$	$0.008 \pm 0.003$	S: $Yb_{0.8}Ga_{0.2}InO_3$	$0.014 \pm 0.005$

The catalysts having Gd and Yb as rare earth ions have shown worse performances than their counterparts with La and Y. Such differences may be due to their particular electronic configurations. In fact,  $Gd^{+3}$  and  $Yb^{+3}$  ions have 4f orbitals that are partially full. Such electrons may favor processes of recombinations of oppositely charged particles and hinder the redox reactions that should take place on the surface of the catalyst [45,46]. The lanthanum(III) and yttrium(III) ions have the peripheral d and f orbitals that are completely empty and do not have unpaired electrons. The catalysts with yttrium are better in producing  $H_2$  than those having lanthanum, probably because Y is a stronger reducing agent than La. Moreover, as far as the crystal structures of the photocatalysts are concerned, the pseudo-hexagonal  $YInO_3$  gives rise to a narrower band gap (315 nm) in comparison with the orthorhombic  $LaInO_3$  (281 nm) and a larger dipole moment, arising from a greater lattice distortion of

YInO<sub>3</sub> compared with LaInO<sub>3</sub>. Such properties may promote the separation of the photo-excited charges, resulting in a higher photocatalytic activity.

### 3.3. Hydrogen Production by Sonolysis in Absence of Photocatalysts

The efficiency of a sonochemical reaction depends on many parameters, such as the frequency of the ultrasound waves, the intensity of the irradiation, the geometry of the reactor, the bulk temperature, the volume of the liquid, *etc.* [47,48]. In this work, we have tested the effect of few parameters in the sonochemical production of hydrogen, like (i) the composition of the liquid; (ii) the total volume of the solution; and (iii) the intensity of ultrasounds.

#### 3.3.1. Effect of the Chemical Composition of the Solution

First, the sonochemical reaction was performed in 300 mL of sheer water, sheer ethanol and ethanol/water (20% vol) mixture without any photocatalyst. The rates of hydrogen production are reported in Table 3.

**Table 3.** Rate of hydrogen production ( $\mu\text{moles/h}$ ) in sonolysis experiments in 300 ml of water, ethanol and ethanol/water (20% vol) mixture irradiated by the 38 kHz piezoelectric transducer without catalysts. The uncertainties have been estimated by calculating the standard deviation of two or more experiments.

Solution	$\mu\text{moles}(\text{H}_2)/\text{h}$
Water	$80 \pm 2$
Ethanol	$5.5 \pm 0.2$
Ethanol/water (20% vol)	$112 \pm 3$

The rate of hydrogen production by sonolysis of sheer water is almost fifteen times larger than that obtained from sheer ethanol. A further improvement has been achieved by adding ethanol to water. In a mixture of ethanol in water (20% in volume), the rate of hydrogen production was 1.4 faster than in sheer water (see Table 3). It is well known that sonolysis of water [28] produces active radical species such as  $H^\bullet$  and  $\bullet OH$ . Then, the radicals can combine to yield hydrogen and hydrogen peroxide (Equation (4)) or recombine and produce water.



It has been shown [49] that sonolysis of organic liquids yields the same species produced by high-temperature pyrolysis. In fact, in our experiments, we detected the typical pyrolysis products of ethanol, such as acetaldehyde and acetic acid. Moreover, we detected the formation of compounds such as hydrogen and methane. The largest amount of H<sub>2</sub> obtained by us in the sonolysis of the ethanol and water mixture may be explained by considering that ethanol can deplete the concentration of  $\bullet OH$ , limiting the recombination of  $\bullet H$  and  $\bullet OH$  radicals [50].

### 3.3.2. Effect of the Volume of the Solution

After ascertaining that the mixture ethanol in water (20% vol.) is better than sheer solvents, we evaluated the effect of the total volume of the solution. In Figure 4, the rate of hydrogen evolution is plotted as function of the total volume of the mixture. This plot shows a periodic trend and its period is 225 mL. The peaks, centered at about 280 mL, 510 mL and 730 mL, correspond to the resonance liquid levels. It is known [51,52] that the periodic trends arise from the change in the acoustic impedance, which is composed of a pure resistance part and a reactance part. The former increases with increasing liquid height, whereas the latter varies periodically. From our results, the volume of 300 mL, which corresponds to the height of 14 mm, has been selected as the optimum value of volume for our further sonolysis and sono-photolysis experiments.

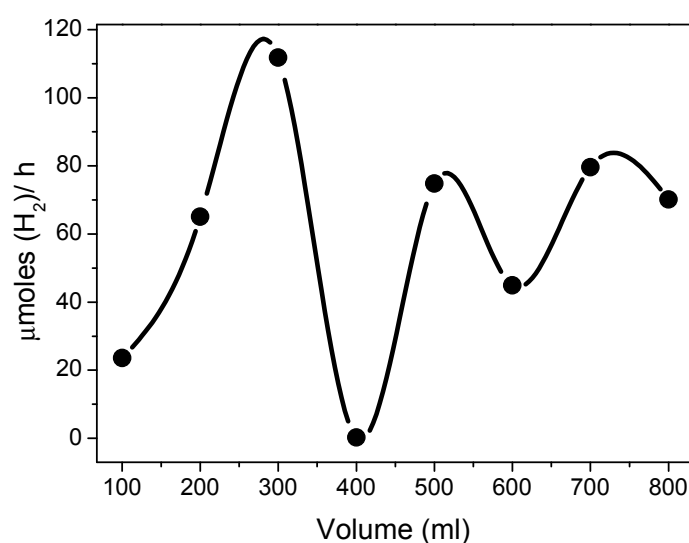


**Figure 4.** Rate of hydrogen production ( $\mu\text{moles}/\text{h}$ ) vs. the volume (expressed in mL) of ethanol in water (20% vol) mixture irradiated by the 38 kHz piezoelectric transducer.

### 3.3.3. The Effect of the Intensity of Ultrasounds

The intensity of irradiation is another important parameter, which affects the efficiency of a sonochemical reaction. Usually, the cavitation activity increases as the acoustic intensity and power of ultrasounds increase. However, such growth is not without any limit: depending on the reactor geometry, the yield of reaction increases up to reach a threshold value, and, after that, it decreases [53–55]. The decrease of the sonochemical efficiency above the threshold value of intensity has been attributed to the formation of a cloud of bubbles near the surface of the transducer, which absorbs and scatters the incident sound waves. Moreover, decoupling losses due to the change in acoustic impedance can affect the efficiency of the process by decreasing the energy transferred to the medium. In order to study the effect of the acoustic power on the sonochemical hydrogen production, we tested different intensities of irradiation. We carried out experiments in 300 mL of an ethanol/water (20% vol) solution by selecting three different levels of power (labeled as minimum, medium and maximum by the instrument producer) of our 38 kHz piezoelectric transducer. As reported in Table 4, the amount of hydrogen grew monotonically as the intensity of ultrasounds increased, without revealing any plateau

or decrease. The level labeled as “maximum” corresponds to a power density of 26 W/dm<sup>3</sup> and to a sonochemical efficiency of  $1.5 \times 10^{-10}$  mol·J<sup>-1</sup> that we determined experimentally as explained in the Experimental section.

**Table 4.** Rate of hydrogen production (μmoles/h) by sonolysis of 300 ml of ethanol/water (20% vol) mixture irradiated by the 38 kHz piezoelectric transducer at its minimum, medium and maximum power.

Power	μmoles(H <sub>2</sub> )/h
Minimum	0
Medium	18.3 ± 0.5
Maximum	112 ± 3

### 3.4. Hydrogen Production by Sonolysis and Sonophotolysis in the Presence of S:Y<sub>0.8</sub>Ga<sub>0.2</sub>InO<sub>3</sub>

Based on the results described in the previous paragraphs, we carried out the experiments of sonolysis and sonophotolysis by irradiating 300 ml of a ethanol/water (20% vol) solution with ultrasound waves of 38 kHz frequency, at the maximum intensity of irradiation, and in the presence of 0.4 g of S:Y<sub>0.8</sub>Ga<sub>0.2</sub>InO<sub>3</sub>. The results are reported in Table 5. If we compare the rate of hydrogen production by sonolysis in the presence of 0.4 g of catalyst (Table 5) with that without catalyst, we see that there are not appreciable differences. On the other hand, when we turn the light on, under the action of ultrasound waves, we detect an interesting synergetic effect of the two types of energies. The extent of synergy may be quantified [36] as the normalized difference between the decomposition rate constants obtained under sonophotocatalysis ( $k_{US+h\nu+Cat}$ ) and the sum of those obtained under separate photocatalysis ( $k_{h\nu+Cat}$ ) and sonocatalysis ( $k_{US+Cat}$ ) (Equation (5)):

$$Synergy = \frac{k_{(US+h\nu+Cat)} - (k_{(h\nu+Cat)} + k_{(US+Cat)})}{k_{(US+h\nu+Cat)}} \quad (5)$$

**Table 5.** Rate of H<sub>2</sub> production (μmol/h) for a suspension of 0.4 g of S:Y<sub>0.8</sub>Ga<sub>0.2</sub>InO<sub>3</sub> in 300 ml ethanol/water (20 vol%) measured in photocatalytic, sonocatalytic and sonophotocatalytic experiments. The synergy value has been calculated by using Equation (5) and its uncertainty by using the formula of propagation of the maximum absolute error.

Sample	Photolysis μmol/h	Sonolysis μmol/h	Sonophotolysis μmol/h	Synergy
S:Y <sub>0.8</sub> Ga <sub>0.2</sub> InO <sub>3</sub>	1.0 ± 0.4	107 ± 3	125 ± 4	0.13 ± 0.05

In our case, we found a synergy of 0.13 that is in agreement with what we found in our previous experiments [29]. Such synergistic effect may be due to different factors. Acoustic cavitations produce particle breakdown with a consequent size reduction and surface area enhancement of the catalyst (as detected by Scanning Electron Microscopy) improving its photocatalytic activity. Water and ethanol degradation species, produced photochemically, can provide extra nuclei for bubble formation. Last but not the least, the ultrasound waves exert a stirring effect into the reactive media. The stirring effect

lifts the particles of the catalyst from the bottom of the reactor up to the top part of the solution and speed up the mass transport between liquid and solid particles.

#### 4. Conclusions

This study shows that the synergy between UV-visible electromagnetic radiation and ultrasound waves in producing hydrogen from a water/ethanol mixture in the presence of heterogeneous catalyst is a promising process in energy research. As photocatalysts, we have used solid solutions of oxides having the  $\text{Ln}_{0.8}\text{Ga}_{0.2}\text{InO}_3$  as formula, with  $\text{Ln} = \text{La}, \text{Y}, \text{Yb}, \text{Gd}$ . The most active was that with Y after doping by sulphur atoms. Then, we have optimized few conditions of the sonolysis experiments, like the composition and the volume of the water solution, and the power of the 38 kHz piezoelectric transducer. We found that an ethanol/water (20% vol.) mixture is a good solution for  $\text{H}_2$  production rather than sheer water or sheer ethanol. Ethanol was chosen because it may be obtained by biomass fermentation in the prospect of a renewable hydrogen economy. Furthermore, second generation technologies allow for the production of bioethanol from non-food sources such as lignocellulosic biomass and agricultural residues [56,57]. Finally, we found that the hybrid action of light and ultrasound waves favors an appreciable synergistic effect in  $\text{H}_2$  production. The final goal of this research is getting hydrogen with a net energy balance: the content of the energy coming from the hydrogen produced by sonophotocatalysis must be greater than the energy spent in the overall process. The results achieved in this work are a step forward with respect to those described in our previous work [29]; nevertheless, further improvements are needed to reach our final goal. For instance, we need to improve the activity of our catalysts by changing their chemical composition and controlling their morphology. We need to test other frequencies of our piezoelectric transducer and optimize the related ultrasounds-solution coupling. We need to optimize the ethanol/water ratio and test other solvents; we also need to design a renewable way to produce the electric power that feeds our piezoelectric transducer, for example by solar panels. We are going to carry out further experiments to approach our goal.

#### Acknowledgments

The financial support from the Ministero per l'Università e la Ricerca Scientifica e Tecnologica (Rome, Italy), the University of Perugia [PRIN 2010-2011, 2010FM738P], the Centro Interuniversitario di Ricerca sull'Inquinamento da Agenti Fisici (C.I.R.I.A.F.) and the Istituto Nazionale di Fisica Nucleare (I.N.F.N.) are gratefully acknowledged.

#### Author Contributions

Marta Penconi collected the data and wrote a first draft of the paper; Federico Rossi designed the sono-photo-catalytic experiments and contributed to the final version of the manuscript; Fausto Ortica contributed to the final version of the manuscript; Fausto Elisei contributed to the final version of the manuscript; Pier Luigi Gentili designed the compositions of the catalysts, analyzed the data and wrote the final version of the paper.

## Conflicts of Interest

The authors declare no conflict of interest.

## References

1. Bockris, J.O'M. The hydrogen economy: Its history. *Int. J. Hydrogen Energy* **2013**, *38*, 2579–2588.
2. Hema Krishna, R. Review of research on production methods of hydrogen: Future fuel. *Eur. J. Biotechnol. Biosci.* **2013**, *1*, 84–93.
3. Rossi, F.; Nicolini, A. Experimental investigation on a novel electrolyte configuration for cylindrical Molten Carbonate Fuel Cells. *J. Fuel Cell Sci. Technol.* **2011**, *8*, 051012.
4. Cotana, F.; Rossi, F.; Nicolini, A. A new geometry high performance small power MCFC. *J. Fuel Cell Sci. Technol.* **2004**, *1*, 25–29.
5. Rossi, F.; Nicolini, A. A cylindrical small size Molten Carbonate Fuel Cell: Experimental investigation on materials and improving performance solutions. *Fuel Cells* **2009**, *9*, 170–177.
6. Rossi, F.; Nicolini, A. Ethanol reforming for supplying Molten Carbonate Fuel Cells. *Int. J. Low-Carbon Technol.* **2013**, *8*, 140–145.
7. Rossi, F.; Nicolini, A.; di Profio, P. Small size cylindrical Molten Carbonate Fuel Cells and future approaches for decreasing working temperature. *ECS Trans.* **2008**, *12*, 455–466.
8. Kudo, A.; Miseki, Y. Heterogeneous photocatalyst materials for water splitting. *Chem. Soc. Rev.* **2009**, *38*, 253–278.
9. Abe, R. Recent progress on photocatalytic and photoelectrochemical water splitting under visible light irradiation. *J. Photochem. Photobiol. C* **2010**, *11*, 179–209.
10. Chen, X.; Shen, S.; Guo, L.; Mao, S.S. Semiconductor-based photocatalytic hydrogen generation. *Chem. Rev.* **2010**, *110*, 6503–6570.
11. Maeda, K. Photocatalytic water splitting using semiconductor particles: History and recent developments. *J. Photochem. Photobiol. C* **2011**, *12*, 237–268.
12. Ismail, A.A.; Bahnemann, D.W. Photochemical splitting of water for hydrogen production by photocatalysis: A review. *Sol. Energy Mater. Solar Cells* **2014**, *128*, 85–101.
13. Sakata, T.; Kawai, T.; Heterogeneous photocatalytic production of hydrogen and methane from ethanol and water. *Chem. Phys. Lett.* **1981**, *80*, 341–344.
14. Gentili, P.L.; Rossi, F.; Penconi, M.; Ortica, F.; Elisei, F. Hydrogen production through sono-photolysis of water in the presence of solid solutions of metal oxides as photocatalysts. Expert Commentary. In *Hydrogen Production: Prospects and Processes*; Honnery, D.R., Moriarty, P., Eds.; Nova Science Publishers, Inc.: New York, NY, USA, 2011; pp. 413–422.
15. Kudo, A.; Mikami, I. Photocatalytic activities and photophysical properties of Ga<sub>2-x</sub>In<sub>x</sub>O<sub>3</sub> solid solution. *J. Chem. Soc. Faraday Trans.* **1998**, *94*, 2929–2932.
16. Maeda, K.; Domen, K. Solid solution of GaN and ZnO as a stable photocatalyst for overall water splitting under visible light. *Chem. Mater.* **2010**, *22*, 612–623.
17. Ouyang, S.; Ye, J.  $\beta$ -AgAl<sub>1-x</sub>Ga<sub>x</sub>O<sub>2</sub> solid-solution photocatalysts: continuous modulation of electronic structure toward high-performance visible-light photoactivity. *J. Am. Chem. Soc.* **2011**, *133*, 7757–7763.

18. Xu, M.; Zai, J.; Yuan, Y.; Qian, X. Band gap-tunable  $(\text{CuIn})_x\text{Zn}_{2(1-x)}\text{S}_2$  solid solutions: Preparation and efficient photocatalytic hydrogen production from water under visible light without noble metals. *J. Mater. Chem.* **2012**, *22*, 23929–23934.
19. Asahi, R.; Morikawa, T.; Ohwaki, T.; Aoki, K.; Taga, Y. Visible-light photocatalysis in nitrogen-doped titanium oxides. *Science* **2001**, *293*, 269–271.
20. Umebayashi, T.; Yamaki, T.; Itoh, V.; Asai, K. Band gap narrowing of titanium dioxide by sulfur doping. *Appl. Phys. Lett.* **2002**, *81*, 454–456.
21. Ohno, T.; Tsubota, T.; Toyofuku, M.; Inaba, R. Photocatalytic activity of a  $\text{TiO}_2$  photocatalyst doped with  $\text{C}^{4+}$  and  $\text{S}^{4+}$  ions having a rutile phase under visible light. *Catal. Lett.* **2004**, *98*, 255–258.
22. Van Sark, W.G.J.H.M.; de Wild, J.; Rath, J.K.; Meijerink, A.; Schropp, R.E.I. Upconversion in solar cells. *Nanoscale Res. Lett.* **2013**, doi:10.1186/1556-276X-8-81.
23. Cheng, Y.Y.; Fückel, B.; MacQueen, R.W.; Khoury, T.; Clady, R.G.C.R.; Schulze, T.F.; Ekins-Daukes, N.J.; Crossley, M.J.; Stannowski, B.; Lips, K.; *et al.* Improving the light-harvesting of amorphous silicon solar cells with photochemical upconversion. *Energy Environ. Sci.* **2012**, *5*, 6953–6959.
24. Penconi, M.; Ortica, F.; Elisei, F.; Gentili, P.L. New molecular pairs for low power non-coherent triplet-triplet annihilation based upconversion: Dependence on the triplet energies of sensitizer and emitter. *J. Lumin.* **2013**, *135*, 265–270.
25. Penconi, M.; Gentili, P.L.; Massaro, G.; Elisei, F.; Ortica, F. A triplet-triplet annihilation based up-conversion process investigated in homogeneous solutions and oil-in-water microemulsions of a surfactant. *Photochem. Photobiol. Sci.* **2014**, *13*, 48–61.
26. Suslick, K.S. Sonocatalysis. Available online: <http://www.scs.illinois.edu/suslick/documents/HBHetCat.pdf> (accessed on 10 July 2015).
27. Joseph, C.G.; Li Puma, G.; Bono, A.; Krishnaiah, D. Sonophotocatalysis in advanced oxidation process: A short review. *Ultrason. Sonochem.* **2009**, *16*, 583–589.
28. Harada, H. Sonophotocatalytic decomposition of water using  $\text{TiO}_2$  photocatalyst. *Ultrason. Sonochem.* **2001**, *8*, 55–58.
29. Gentili, P.L.; Penconi, M.; Ortica, F.; Cotana, F.; Rossi, F.; Elisei, F. Synergistic effects in hydrogen production through water sonophotolysis catalyzed by new  $\text{La}_{2x}\text{Ga}_{2y}\text{In}_{2(1-x-y)}\text{O}_3$  solid solutions. *Int. J. Hydrogen Energy* **2009**, *34*, 9042–9049.
30. Durán, A.; Monteagudo, J.M.; Sanmartín, I.; García-Díaz, A. Sonophotocatalytic mineralization of antipyrine in aqueous solution. *Appl. Catal. B* **2013**, *138–139*, 318–325.
31. Jagannathan, M.; Grieser, F.; Ashokkumar, M. Sonophotocatalytic degradation of paracetamol using  $\text{TiO}_2$  and  $\text{Fe}^{3+}$ . *Sep. Purif. Technol.* **2013**, *103*, 114–118.
32. Anju, S.G.; Yesodharan, S.; Yesodharan, E.P. Zinc oxide mediated sonophotocatalytic degradation of phenol in water. *Chem. Eng. J.* **2012**, *189–190*, 84–93.
33. Cheng, Z.; Quan, X.; Xiong, Y.; Yang, L.; Huang, Y. Synergistic degradation of methyl orange in an ultrasound intensified photocatalytic reactor. *Ultrason. Sonochem.* **2012**, *19*, 1027–1032.
34. Sekiguchi, K.; Sasaki, C.; Sakamoto, K. Synergistic effects of high-frequency ultrasound on photocatalytic degradation of aldehydes and their intermediates using  $\text{TiO}_2$  suspension in water. *Ultrason. Sonochem.* **2011**, *18*, 158–163.

35. Chen, Y.C.; Vorontsov, A.V.; Smirniotis, P.G. Enhanced photocatalytic degradation of dimethyl methylphosphonate in the presence of low-frequency ultrasound. *Photochem. Photobiol. Sci.* **2003**, *2*, 694–698.
36. Mrowetz, M.; Pirola, C.; Selli, E. Degradation of organic water pollutants through sonophotocatalysis in the presence of TiO<sub>2</sub>. *Ultrason. Sonochem.* **2003**, *10*, 247–254.
37. Gentili, P.L.; Penconi, M.; Costantino, F.; Sassi, P.; Ortica, F.; Rossi, F.; Elisei, F. Structural and photophysical characterization of some La<sub>2x</sub>Ga<sub>2y</sub>In<sub>2z</sub>O<sub>3</sub> solid solutions, to be used as photocatalysts for H<sub>2</sub> production from water/ethanol solutions. *Sol. Energy Mater. Sol. Cells* **2010**, *94*, 2265–2274.
38. Gentili, P.L.; Clementi, C.; Romani, A. Ultraviolet-Visible Absorption and Luminescence Properties of Quinacridone-Barium Sulfate Solid Mixtures. *Appl. Spectrosc.* **2010**, *64*, 923–929.
39. Koda, S.; Kimura, T.; Kondo, T.; Mitome, H. A standard method to calibrate sonochemical efficiency of an individual reaction system. *Ultrason. Sonochem.* **2003**, *10*, 149–156.
40. Ruiz-Trejo, E.; Tavizón, G.; Arroyo-Landeros, A. Structure, point defects and ion migration in LaInO<sub>3</sub>. *J. Phys. Chem. Solid* **2003**, *64*, 515–521.
41. Park, H.M.; Lee, H.J.; Park, S.H.; Yoo, H.I. Lanthanum indium oxide from X-ray powder diffraction. *Acta Cryst.* **2003**, *C59*, i131–i132.
42. Smith, A.E.; Mizoguchi, H.; Delaney, K.; Spaldin, N.A.; Sleight, A.W.; Subramanian, M.A. Mn<sup>3+</sup> in trigonal bipyramidal coordination: A new blue chromophore. *J. Am. Chem. Soc.* **2009**, *131*, 17084–17086.
43. Kuo, D.H.; Huang, K.C. Phase composition and properties of solid solutions of GdFeO<sub>3</sub>–GdInO<sub>3</sub> bulks. *Ceram. Int.* **2008**, *34*, 1503–1507.
44. Pistorius, C.W.F.T.; Kruger, G.J. Stability and structure of noncentrosymmetric hexagonal LnInO<sub>3</sub> (Ln = Eu, Gd, Tb, Dy, Ho, Y). *J. Inorg. Nucl. Chem.* **1976**, *38*, 1471–1475.
45. Uno, M.; Kosuga, A.; Okui, M.; Horisaka, K.; Muta, H.; Kurosaki, K.; Yamanaka, S. Photoelectrochemical study of lanthanide zirconium oxides, Ln<sub>2</sub>Zr<sub>2</sub>O<sub>7</sub> (Ln = La, Ce, Nd and Sm). *J. Alloys Compd.* **2006**, *420*, 291–297.
46. Machida, M.; Murakami, S.; Kijima, T.; Matsushima, S.; Arai, M. Photocatalytic property and electronic structure of lanthanide tantalates, LnTaO<sub>4</sub> (Ln = La, Ce, Pr, Nd, and Sm). *J. Phys. Chem. B* **2001**, *105*, 3289–3294.
47. Sutkar, V.S.; Gogate, P.R. Design aspects of sonochemical reactors: Techniques for understanding cavitation activity distribution and effect of operating parameters. *Chem. Eng. J.* **2009**, *155*, 26–36.
48. Thompson, L.H.; Doraiswamy, L.K. Sonochemistry: Science and engineering. *Ind. Eng. Chem. Res.* **1999**, *38*, 1215–1249.
49. Misik, V.; Riesz, P. Recent applications of EPR and spin trapping to sonochemical studies of organic liquids and aqueous solutions. *Ultrason. Sonochem.* **1996**, doi:10.1016/S1350-4177(96)00023-5.
50. Sasikala, R.; Jayakumar, O.D.; Kulshreshtha, S.K. Enhanced hydrogen generation by particles during sonochemical decomposition of water. *Ultrason. Sonochem.* **2007**, *14*, 153–156.
51. Asakura, Y.; Nishida, T.; Matsuoka, T.; Koda, S. Effects of ultrasonic frequency and liquid height on sonochemical efficiency of large-scale sonochemical reactors. *Ultrason. Sonochem.* **2008**, *15*, 244–250.

52. Wu, C.; Nakagawa, N.; Sekiguchi, Y. Observation of multibubble phenomena in an ultrasonic reactor. *Exp. Therm. Fluid Sci.* **2007**, *31*, 1083–1089.
53. Sivakumar, M.; Pandit, A.B. Ultrasound enhanced degradation of Rhodamine B: optimization with power density. *Ultrason. Sonochem.* **2001**, *8*, 233–240.
54. Ondruschka, B.; Lifka, J.; Hofmann, J. Aquasonolysis of Ether—Effect of Frequency and Acoustic Power of Ultrasound. *Chem. Eng. Technol.* **2000**, *23*, 588–592.
55. Gutierrez, M.; Henglein, A. Chemical action of pulsed ultrasound: observation of an unprecedented intensity effect. *J. Phys. Chem.* **1990**, *94*, 3625–3628.
56. Sarkar, N.; Ghosh, S.K.; Bannerjee, S.; Aikat, K. Bioethanol production from agricultural wastes: An overview. *Renew. Energy* **2012**, *37*, 19–27.
57. Cotana, F.; Cavalaglio, G.; Gelsia, M.; Nicolini, A.; Coccia, V.; Petrozzi, A. Production of bioethanol in a second generation prototype from pine wood chips. *Energy Procedia* **2014**, *45*, 42–51.

© 2015 by the authors; licensee MDPI, Basel, Switzerland. This article is an open access article distributed under the terms and conditions of the Creative Commons Attribution license (<http://creativecommons.org/licenses/by/4.0/>).